Acta Crystallographica Section D
Biological Crystallography
ISSN 0907-4449

Real-space molecular-dynamics structure refinement

Zhi Chen,[a] Eric Blanc[a]† and Michael S. Chapman[a,b]*

[a]Institute of Molecular Biophysics, Florida State University, Tallahassee, FL 32306-4380, USA, and [b]Department of Chemistry, Florida State University, Tallahassee, FL 32306-4380, USA

† Current address: Global Phasing Ltd, Sheraton House, Castle Hill Business Park, Cambridge CB3 0AX, England.

Correspondence e-mail: chapman@sb.fsu.edu

Received 23 March 1998
Accepted 17 August 1998

Real-space targets and molecular-dynamics search protocols have been combined to improve the convergence of macromolecular atomic refinement. This was accomplished by providing a local real-space target function for the molecular-dynamics program *X-PLOR*. With poor isomorphous replacement experimental phases, molecular dynamics does not improve real-space refinement. However, with high-quality anomalous diffraction phases convergence is improved at the start of refinement, and torsion-angle real-space molecular dynamics performs better than other available least-squares or maximum-likelihood methods in real or reciprocal space. It is shown that the improvements result from an optimization method that can escape local minima and from a reduction of overfitting through the implicit use of phases and through use of a local refinement in which errors in remote parts of the structure cannot be mutually compensating.

1. Introduction

The most common macromolecular crystallographic refinement involves restrained optimization of the agreement between diffraction amplitudes calculated from an atomic model and those derived from the experimental data (Jensen, 1985). Stereochemical restraints are introduced either by optimizing the agreement with ideal geometries (Engh & Huber, 1991; Hendrickson, 1985; Waser, 1963) or (as in this work) through minimization of an empirical estimate of the configurational potential energy, $E_{\rm chem}$ (Brünger *et al.*, 1987; Levitt, 1974). Structural refinement then becomes minimization of the objective function

$$E = E_{\rm chem} + wE_{\rm xray},$$

where

$$E_{\rm xray}(F) = \sum_{h}[|\mathbf{F}_c(\mathbf{h})| - |\mathbf{F}_o(\mathbf{h})|]^2 \qquad (1)$$

and $\mathbf{F}_o$ and $\mathbf{F}_c$ are the experimental and scaled calculated structure amplitudes for reflection **h**. Equation (1) shows a least-squares target, but analogous maximum-likelihood targets have recently also shown promise (Murshudov *et al.*, 1997; Pannu & Read, 1996). Methods used to find an optimal structure are either one of the gradient-descent methods (see Tronrud, 1992) or use a protocol such as simulated-annealing (SA) optimization, which enables the structure to leave a local minimum, combined with molecular-dynamics (MD) sampling of conformational space (Brünger *et al.*, 1987). SA and MD methods increase the convergence radius of atomic refinement, because the surface of the objective function has many local minima in which gradient-descent methods can stall as they may be unable to pass through stereochemically unfa-

vorable configurations to explore, for example, alternative rotamers. Constraining bond lengths and angles by changing torsion angles in MD instead of the Cartesian atomic coordinates increases the radius of reciprocal-space refinement to ~1.7 Å (Brünger & Rice, 1997).

Although reciprocal-space $E_{\rm xray}$ terms are currently preferred, early refinements used a real-space target (Diamond, 1971),

$$E_{\rm xray}(\rho) = \int (\rho_c - \rho_o)^2 {\rm d}v, \qquad (2)$$

where is it now a difference between observed and calculated electron density over molecular volume v that is optimized. Although Diamond (1971) noted a potentially wide convergence radius, real-space methods have been largely superseded by reciprocal-space methods owing to the implicit dependence of real-space methods upon the phases used to calculate the electron-density map, which are often much less accurate than the diffraction amplitudes. Real-space refinement continues to be applied in several niches, such as the refinement of (virus) structures with excellent phase and map quality arising from high non-crystallographic symmetry (Jones & Liljas, 1984) and as a tool to assist the fitting of rigid fragments to electron density during interactive model-building (for a review, see Jones & Kjeldgaard, 1997). Recent methodological advances have expanded its application as an aide in model building (Blanc & Chapman, 1997), as a complement to reciprocal-space methods to improve convergence (Chapman & Blanc, 1997) in protein structure refinement and as an efficient alternative for the complete refinement of virus structures (Chapman & Rossmann, 1996). The improvements include the incorporation of modern stereochemical restraints and the use of an atomic electron-density function which explicitly accounts for the resolution limits of the electron-density map (Chapman, 1995),

$$\rho_c(r) = 4\pi O \int_{\rm low\ resolution}^{\rm high\ resolution} g(r^*) r^{*2} \frac{\sin(2\pi r r^*)}{2\pi r r^*} {\rm d}r^*, \qquad (3)$$

where O is the occupancy and g is the atomic scattering factor, which is dependent on the resolution r^* and incorporates isotropic thermal vibration factors.

As in earlier implementations, the newer real-space refinements optimized the structure by gradient-descent methods (Tronrud, 1992). This work examines the potential of combining two methods that have robust convergence properties – namely, real-space targets and molecular-dynamics optimization. The potential application of such methodology has broadened considerably recently with the availability of accurate macromolecular phases from multiwavelength anomalous diffraction (MAD) methods (Hendrickson & Ogata, 1997).

2. Methods

Real-space MD was implemented by programming an alternative target function for *X-PLOR* (Brünger, 1992*b*) that provides the option of substituting (2) for $E_{\rm xray}$ in (1). A prior implementation of a real-space target (Chapman, 1995) was adapted so that input and output was compatible with *X-PLOR* programs, data files and control scripts. The target value and its derivatives with respect to the atomic parameters are calculated with the new module and passed back to *X-PLOR*. Thus, all methods of optimization that have been applied in reciprocal space (Brünger *et al.*, 1997) can now be applied in real space, including torsion-angle or Cartesian MD (and conjugate-gradient optimization).

Initial tests used simulated structure amplitudes, phases and maps calculated from α-amylase inhibitor (Pflugrath *et al.*, 1989) between 17 and 2 Å resolution. Starting models were perturbed by varying amounts using molecular dynamics at 600 K followed by energy minimization, all in the absence of an $E_{\rm xray}$ term. The test-refinement protocol involved 4 ps of torsion-angle MD at 8000 K (now including an $E_{\rm xray}$ term) and 0.2 ps of quenching at 300 K in Cartesian space, followed by conjugate-gradient energy minimization. Slow-cooling protocols were tested but, as in reciprocal-space torsion-angle refinements (Rice & Brünger, 1994), they proved to be inferior to rapid quenching and are not considered further. With phases calculated directly from the correct structure, a starting model with 1.43 Å r.m.s. backbone error is refined to an error of 0.1 Å. The convergence radius is 3.6 Å, as defined by the maximal backbone perturbation that can still be refined to approximate the correct structure. With an omit map (Bhat, 1988) calculated from the perturbed model, the radius of convergence was 0.6 Å, indicating dependence of the method upon the availability of experimental phases.

Real-space torsion-angle molecular dynamics (RSTAMD) was tested in two systems with actual crystallographic data. HMG CoA reductase represented poor experimental phases and mannose binding protein A (MBPA) represented high-quality experimental phases. HMG CoA reductase exemplified a large protein structure determination in which poor multiple isomorphous replacement (MIR) phases were improved by the application of non-crystallographic symmetry (NCS) in the actual structure determination (Lawrence *et al.*, 1995). For the current tests, the NCS was ignored and the unrefined model of Lawrence *et al.* was refined against a barely interpretable MIR map.

MBPA exemplified high-quality MAD phasing (Burling *et al.*, 1996). The starting model was based on a 2.3 Å resolution homologous complex with a different lanthanide ion (Weis *et al.*, 1991), with remodeling of seven disordered terminal residues into the 1.8 Å resolution MAD map (Burling *et al.*, 1996), deletion of solvent molecules, resetting all B factors to 15 Å, stereochemical regularization and rigid-body reciprocal-space refinement against the 1.8 Å cryodiffraction data (Burling *et al.*, 1996). Additional tests started with the 1.8 Å resolution final refined structure (Burling *et al.*, 1996).

The refinement methods that were compared using MBPA included the following. All methods were as implemented in *X-PLOR* (Brünger, 1992*b*). When molecular dynamics was used, the torsion-angle implementation (Rice & Brünger, 1994) was used and was followed by conjugate-gradient minimization of the objective function.

Table 1
Refinement of a 2.3 Å MBPA structure (derived from Weis *et al.*, 1991) against 1.8 Å diffraction data (Burling *et al.*, 1996) by several methods (further described in the text).

When used, phase restraints were given weight equal to amplitude restraints.

Method	Target	Equation	Optimization	R.m.s. deviation (Å)		R^{work}	R^{free}
				Backbone	Overall		
Published 1.8 Å structure†				0.000	0.000	0.299	0.289
Starting model‡				0.282	0.792	0.349	0.345
(i)	$E_{xray}(\rho)$	2	Molecular dynamics	0.123	0.640	0.313§	0.312§
(i*b*)	$E_{xray}(\rho)$	2 With local improvement¶	Molecular dynamics	0.123	0.524	0.313	0.311
(ii)	$E_{xray}(\rho)$	2	Gradient descent	0.153	0.706	0.317	0.311
(iii)	E_{xray}(F)	1	Molecular dynamics	0.183	0.704	0.289	0.329
(iv)	E_{xray}(F)	1	Gradient descent	0.185	0.733	0.304	0.325
(v)	$E_{xray}(\rho)$ then $E_{xray}(F)$	2, 1	Molecular dynamics	0.112	0.627	0.302	0.313
(vi)	E_{xray}(A,B)	4	Molecular dynamics	0.165	0.669	0.316	0.323
(vi*b*)	E_{xray}(A,B)	4 With f.o.m. weighting	Molecular dynamics	0.156	0.657	0.310	0.318
(vii)	E_{xray}(F,φ)	5	Molecular dynamics	0.175	0.689	0.286	0.327
(viii)	$E^{ML}_{xray}[P(\lvert\mathbf{F}_o\rvert, \lvert\mathbf{F}_c\rvert)]$	6	Molecular dynamics	0.167	0.716	0.313	0.325
(ix)	$E^{ML}_{xray}[P(\lvert\mathbf{F}_o\rvert, \lvert\mathbf{F}_c\rvert)]$	6	Gradient descent	0.173	0.730	0.315	0.327
(x)	$E^{ML}_{xray}[P(\lvert\mathbf{F}_o\rvert, \lvert\mathbf{F}_c\rvert)]$	6 Plus phase restraints	Molecular dynamics	0.127	0.688	0.313	0.319

† Less solvent and with B = 15. ‡ Modified 2.3 Å structure. § Standard deviations for R^{work} and R^{free} were ±0.001 and ± 0.004, respectively, as calculated for ten repeated refinements with different non-overlapping test sets. ¶ The 13 regions with worst real-space correlation factor were refined further separately with a local real-space protocol.

(i) Real-space least-squares MD refinement of $E_{xray}(\rho)$ (2). The real-space targets used here, and in methods (ii) and (v) are described in detail in §1.

(i*b*) The amino acids with the worst agreement with the electron density were further locally refined, as indicated by the correlation coefficient (Jones *et al.*, 1991; calculated according to Zhou *et al.*, 1998).

(ii) Real-space least-squares conjugate-gradient refinement of $E_{xray}(\rho)$ (2) without MD.

(iii) Reciprocal-space least-squares MD refinement of $E_{xray}(F)$ (1). This corresponds to the mode of refinement for which *X-PLOR* is most commonly used (Brünger *et al.*, 1987).

(iv) Reciprocal-space least-squares conjugate-gradient refinement of $E_{xray}(F)$ (1) without MD. This would correspond to a 'conventional' non-dynamics refinement.

(v) Real-space least-squares MD refinement of $E_{xray}(\rho)$ (2) followed by reciprocal-space least-squares MD refinement of $E_{xray}(F)$ (1).

(vi) Vector-residual (Arnold & Rossmann, 1988) least-squares MD refinement,

$$E_{xray}(A,B) = \sum_{\mathbf{h}} m(\mathbf{h})\{[A_c(\mathbf{h}) - A_o(\mathbf{h})]^2 + [B_c(\mathbf{h}) - B_o(\mathbf{h})]^2\}, \quad (4)$$

where (A, B) are the real and imaginary components of the structure factor and m is the figure of merit.

(vii) Phase (φ) restrained (Rees & Lewis, 1983) least-squares MD refinement,

$$E_{xray}(F,\varphi) = \sum_{\mathbf{h}}[\lvert\mathbf{F}_c(\mathbf{h})\rvert - \lvert\mathbf{F}_o(\mathbf{h})\rvert]^2 + w_\varphi \sum_{\mathbf{h}} f[\varphi_c(\mathbf{h}) - \varphi_o(\mathbf{h})]. \quad (5)$$

[Methods (vi) and (vii) can be considered pseudo-real-space methods in that they approximate the effect of a real-space target with computation in reciprocal-space.]

(viii) Maximum-likelihood (Pannu & Read, 1996) MD refinement (Adams *et al.*, 1997),

$$E^{ML}_{xray}[P(\lvert\mathbf{F}_o\rvert, \lvert\mathbf{F}_c\rvert)] = -\sum_{\mathbf{h}} \log\{P[\lvert\mathbf{F}_o(\mathbf{h})\rvert, \lvert\mathbf{F}_c(\mathbf{h})\rvert]\} \simeq \textstyle\sum_{\mathbf{h}}(1/\sigma^2_{ML})[\lvert\mathbf{F}_o(\mathbf{h})\rvert - \langle\lvert\mathbf{F}_o(\mathbf{h})\rvert\rangle]^2, \quad (6)$$

where P is the probability of observing $\mathbf{F}_o$ given a model $\mathbf{F}_c$, σ^2_{ML} is the variance of P and $\langle\mathbf{F}\rangle$ denotes the expected value of $\mathbf{F}$.

(ix) Maximum-likelihood MD refinement with additional phase restraint analogous to method (vii) (Pannu & Read, 1997).

E_{chem} was calculated with the same internal weights and parameters for all refinements. Each protocol was optimized by searching for the weight on E_{xray} that gave the lowest R^{free} for a 3–6% test set (Brünger, 1992*a*). Maps for real-space refinement were figure-of-merit weighted and omitted test-set amplitudes that were replaced by the (unbiased) resolution-shell average amplitude to mitigate the deleterious effects of missing reflections (Chen *et al.*, 1999). Torsion-angle MD involved elevating the temperature to 5000 K for 2 ps, followed by quenching to 300 K for ∼0.1 ps then 100 steps of conjugate-gradient optimization. In all cases, only protein-atom positions were refined – B factors remained fixed at 15 Å^2 and the resolution limits were always 10–1.8 Å.

3. Results and discussion

Application to the least favorable case of poor MIR phases in HMG CoA reductase showed that MD and conjugate-gradient real-space refinement performed near-identically. It was shown previously (Chapman & Blanc, 1997) that for poor phases, real-space refinement enhances but does not supersede reciprocal-space methods when the two are alternated in the initial cycles. Here, it is confirmed that real-space refinement is limited by the poor MIR phases and not the optimi-

Table 2
Further refinement of the 1.8 Å refined MBPA structure in real and reciprocal space.

Method	Target	Equation	Optimization	Phases	Correlation coefficient	R^{work}	R^{free}
Starting model†					0.917	0.196	0.216
(i)	$E_{xray}(\rho)$	2	Molecular dynamics	MAD	0.929	0.216	0.217
(iii)	$E_{xray}(F)$	1	Molecular dynamics	N/A		0.202	0.207
(i)	$E_{xray}(\rho)$	2	Molecular dynamics	Calculated		0.203	0.206

† Published 1.8 Å structure (Burling *et al.*, 1996).

zation algorithm. Thus, least squares and MD are equally effective.

The potential with good phases is graphically illustrated in Fig. 1. Real-space MD, unlike its gradient-descent counterpart, is able to pass through an unfavorable configuration to find the best fit to the electron density. Quantitatively, it is clear from Table 1 that real-space molecular dynamics is the most powerful method for initial refinement when the map quality is good. R^{free} drops about twice as much as with any of the currently available reciprocal-space methods, including maximum likelihood. [Smaller differences between maximum likelihood and least-squares targets are seen here compared with those observed earlier (Pannu & Read, 1996) owing to the high quality 2.3 Å MBPA starting model.] Coordinate error drops about 60% farther for RSTAMD than for the reciprocal-space methods. Real-space gradient descent is intermediate in performance between RSTAMD and reciprocal-space methods. The RSTAMD-refined model has an R^{free} about twice as close to the target model as those produced by reciprocal-space refinements, indicating that some but not all of the changes normally made by manual intervention have been accomplished automatically. Unlike HMG CoA reductase, the benefit of following initial real-space refinement with reciprocal-space refinement is at most marginal, presumably because the phase quality is not limiting at this stage of the MBPA refinement.

At the end of refinement, the indications are different (Table 2). Starting with the published, fully refined 1.8 Å MBPA structure (Burling *et al.*, 1996), additional refinement in real space using the MAD phases yields a structure with R^{free} slightly higher than in reciprocal space (0.217 *versus* 0.207). It is the MAD phases that are limiting, as is shown through substitution of phases calculated from the final model which allows real-space refinement to equal reciprocal-space refinement (R^{free} = 0.206, Table 2). Thus, there comes a point in refinement when the model errors become sufficiently low that phase error limits real-space refinement, and reciprocal-space methods are indicated. With high-quality MAD phases, this point is reached only for the final cycles.

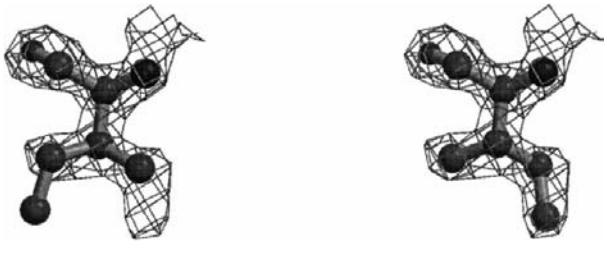

Figure 1
Rotamer correction by real-space molecular dynamics refinement. Ile147 of mannose binding protein A (Burling *et al.*, 1996) was perturbed to an incorrect rotamer using the modeling program *O* (Kleywegt & Jones, 1997). Refinement against the MAD experimental electron density (shown) corrects the rotamer. While this particular type of error might be correctable with the tools in *O* (Kleywegt & Jones, 1997), quick application of the refinement to the whole protein can substantially reduce the number of corrections that need to be made with an interactive modeling program.

While improvements of R^{free} and backbone coordinate error during initial refinement are appreciable, substantial errors remain in side-chain coordinates with all refinement methods (Table 1). Some improvement is made with a new algorithm that is possible using a local method of real-space refinement. The worst amino acids are identified according to correlation between model and experimental electron density (Zhou *et al.*, 1998) and, as individual amino acids, are given additional cycles of RSTAMD. Applied to the 13 worst amino acids, the overall r.m.s. coordinate error is reduced from 0.64 to 0.52 Å (Table 1), but there is little change in the *R* factors because it is a small fraction of the weakest-scattering part of the molecule that is improved. The remaining error is mostly because of the selection of incorrect rotamers, owing to the lack of ordered water molecules in the model and owing to the remaining need to make some corrections interactively rather than through the automatic refinement methods used. The local procedure helps at the initial stages of refinement when all *B* factors are uniform, and the local method enables more appropriate scaling (and refinement) between the more disordered parts of the model and their weak electron density. Such a procedure could also be used to try to automatically fix some of the most egregious errors of a model as highlighted by other (stereochemical) indicators, although there will still be a need for visual inspection to correct, for example, register errors.

Table 1 gives some indications of how real-space refinement helps in all but the final cycles. Although the greatest drop in R^{free} is seen with real-space refinement, the drop in crystallographic R^{work} is less than or equal to the drop using the various reciprocal-space refinements, and substantially less than the commonly used amplitude-based MD refinement. Thus, in real space, overfitting is substantially reduced. Overfitting early in refinement can also be reduced by appropriately accounting for model and data errors in the maximum-likelihood formulation (Pannu & Read, 1996). The source of the improvement with real-space methods is fundamentally different. It is the improvement of the data-to-parameter ratio through the use of implicit phase information and also the use of a local refinement method (see later). In

the case of MBPA, with low model error and high phase accuracy, the reduction of overfitting is greater with real-space methods than with maximum-likelihood methods. The pseudo-real-space methods [(vi), (vi*b*) and (vii)] also incorporate phase information, are the best of the reciprocal-space methods and reduce overfitting somewhat, but not as much as the true real-space algorithm. This may seem counter-intuitive, as there is at least a superficial correspondence of the real- and reciprocal-space operations (Diamond, 1971; Silva & Rossmann, 1985). However, there are differences in the weighting and in the local/global nature of refinement. The closest correspondence is between $E_{\rm xray}(\rho)$ and $E_{\rm xray}(A, B)$ [methods (i) and (vi*b*)], when both incorporate figure-of-merit weighting. The remaining difference between these targets is presumably a consequence of the local nature of real-space refinement *versus* the global nature of all reciprocal-space and *pseudo*-real-space methods. In global methods, all parts of the model move to decrease the discrepancy between F_o and F_c. Atoms may be moved away from their correct locations to reduce discrepancies arising from remote errors in the model (Hodel *et al.*, 1992), an incomplete description of solvent or missing macromolecular atoms. With a local real-space method, these contributions to the overfitting are eliminated, leading to improved refinement at the early stages.

4. Conclusions

Real-space refinement can be significantly enhanced with the addition of molecular-dynamics optimization methods. With high-quality phases and maps, the improvement over other refinement methods is substantial, until phase errors dominate over model errors in the final cycles. With low-quality maps and phases, the method is benign. This suggests a pragmatic approach when the experimental phases are of uncertain quality – do all possible refinement in real-space, then complete refinement in reciprocal space. With the high-quality phases and maps that are increasingly available with anomalous diffraction, the results reported here suggest that real-space refinement will become an increasingly important part of the efficient structure determination of a significant proportion of protein structures.

We thank Temple Burling, Axel Brunger, Martin Lawrence and Cynthia Stauffacher for access to the MBPA and HMG CoA reductase coordinates and diffraction data. This work was supported by the National Science Foundation (BIR94-18741). Modifications to *X-PLOR* that enable real-space molecular-dynamics refinement will be available directly from the authors.

References

Adams, P. D., Pannu, N. S., Read, R. J. & Brünger, A. T. (1997). *Proc. Natl Acad. Sci. USA*, **94**, 5018–5023.
Arnold, E. & Rossmann, M. G. (1988). *Acta Cryst.* A**44**, 270–282.
Bhat, T. N. (1988). *J. Appl. Cryst.* **21**, 279–281.
Blanc, E. & Chapman, M. S. (1997). *J. Appl. Cryst.* **30**, 566–567.
Brünger, A. T. (1992*a*). *Nature (London)*, **355**, 472–475.
Brünger, A. T. (1992*b*). *X-PLOR Version 3.1. A System for X-ray Crystallography and NMR*. New Haven: Yale University Press.
Brünger, A. T., Adams, P. D. & Rice, L. M. (1997). In *NATO Advanced Study Institute on Direct Methods for Solving Macromolecular Structures*, edited by S. Fortier, pp. 149–163. Dordrecht: Kluwer.
Brünger, A. T., Kuriyan, J. & Karplus, M. (1987). *Science*, **235**, 458–460.
Brünger, A. T. & Rice, L. M. (1997). *Methods Enzymol.* **277**, 243–269.
Burling, F. T., Weis, W. I., Flaherty, K. M. & Brünger, A. (1996). *Science*, **271**, 72–77.
Chapman, M. S. (1995). *Acta Cryst.* A**51**, 69–80.
Chapman, M. S. & Blanc, E. (1997). *Acta Cryst.* D**53**, 203–206.
Chapman, M. S. & Rossmann, M. G. (1996). *Acta Cryst.* D**52**, 129–142.
Chen, Z., Blanc, E. & Chapman, M. S. (1999). *Acta Cryst.* D**55**. In the press.
Diamond, R. (1971). *Acta Cryst.* A**27**, 436–452.
Engh, R. A. & Huber, R. (1991). *Acta Cryst.* A**47**, 392–400.
Hendrickson, W. A. (1985). *Methods Enzymol.* **115**, 252–270.
Hendrickson, W. A. & Ogata, C. M. (1997). *Methods Enzymol.* **276**, 494–523.
Hodel, A., Kim, S.-H. & Brünger, A. T. (1992). *Acta Cryst.* A**48**, 851–858.
Jensen, L. H. (1985). *Methods Enzymol.* **115**, 227–234.
Jones, T. A. & Kjeldgaard, M. (1997). *Methods Enzymol.* **277**, 173–208.
Jones, T. A. & Liljas, L. (1984). *Acta Cryst.* A**40**, 50–57.
Jones, T. A., Zou, J.-Y., Cowan, S. W. & Kjeldgaard, M. (1991). *Acta Cryst.* A**47**, 110–119.
Kleywegt, G. J. & Jones, T. A. (1997). *Methods Enzymol.* **277**, 208–230.
Lawrence, C. M., Rodwell, V. M. & Stauffacher, C. V. (1995). *Science*, **268**, 1758–1762.
Levitt, M. (1974). *J. Mol. Biol.* **82**, 393–420.
Murshudov, G., Vagin, A. & Dodson, E. (1997). *Acta Cryst.* D**53**, 240–255.
Pannu, N. S. & Read, R. J. (1996). *Acta Cryst.* A**52**, 659–668.
Pannu, N. S. & Read, R. J. (1997). *NATO Advanced Study Institute on Direct Methods for Solving Macromolecular Structures*, edited by S. Fortier, p. 488. Dortrecht: Kluwer.
Pflugrath, J. W., Wiegand, G., Huber, R. & Vertesey, L. (1989). *J. Mol. Biol.* **189**, 383–386.
Rees, D. C. & Lewis, M. (1983). *Acta Cryst.* A**39**, 94–97.
Rice, L. M. & Brünger, A. T. (1994). *Proteins Struct. Funct. Genet.* **19**, 277–290.
Silva, A. M. & Rossmann, M. G. (1985). *Acta Cryst.* B**41**, 147–157.
Tronrud, D. E. (1992). *Acta Cryst.* A**48**, 912–916.
Waser, J. (1963). *Acta Cryst.* **16**, 1091–1094.
Weis, W. I., Kahn, R., Fourne, R., Drickamer, K. & Hendrickson, W. A. (1991). *Science*, **254**, 1608–1615.
Zhou, G., Wang, J., Blanc, E. & Chapman, M. S. (1998). *Acta Cryst.* D**54**, 391–399.